Point-by-point responses to referee's comments for acp-20130782

Responses Referee #2:

General comments：

This article focuses on Asian terrestrial carbon fluxes using ensemble Kalman filter method adopted by CARBONTRACKER. The important feature is that the authors make use of continuous aircraft dataset obtained by CONTRAIL project in this analysis system. As some previous studies show that the aircraft dataset are significantly available to constrain Asian carbon fluxes. The combination of the analysis method and this observation data is new and this article has a value for publish. However, the authors do not show their analysis results in global scale in this article and this make us difficult to evaluate their analysis system correctly. I recommend comparing their analysis result in global scale with other inversion study for acceptance. Especially comparing with CARBONTRACKER in US or Europe is preferable as the analysis system is almost similar to them.

Response:

Many thanks to the Referee #2 for his/her positive evaluation and useful comments/suggestions. We agree that we should explicitly describe the inverted information of global carbon sinks/source in the paper; otherwise it makes the readers difficult to evaluate the analysis system correctly. We have now added the global analysis results in our revised version. Also, the comparison of our results with CarbonTracker in US or Europe was also added in. *See Table 3 in page 35 and SI Appendix B in page 55-57.*

Table 3. Results of the sensitivity experiments conducted in this study (Pg C yr^{-1})[a]

Inversion ID	Case 1	Case 2	Case 3	Case 4	Case 5	Case 6

Boreal Eurasia	-1.02	-0.96	-1.11	-1.25	-1.03	-0.92
Temperate Eurasia	-0.68	-0.33	-0.70	-0.63	-0.37	-0.36
Tropical Asia	0.15	0.19	0.12	0.08	0.17	0.20
Total Asia	-1.56	-1.09	-1.69	-1.80	-1.23	-1.07
NH land sink	-2.93	-2.64	-3.20	-3.20	-2.79	-2.70
Land	-2.43	-2.24	-3.07	-3.25	-2.65	-2.50
Ocean	-2.08	-2.16	-2.04	-2.05	-2.27	-2.18
Global	-4.50	-4.41	-5.12	-5.30	-4.92	-4.68

[a]The Case 1 (Surface-CONTRAIL) and Case 2 (Surface-Only) run for the period 2006-2010, while Case 3-6 run for the period 2008-2010; detailed discussion on global flux estimates can be found in SI Appendix B.

Supporting Information Appendix B:

Table B1. Global annual average aggregated fluxes for TransCom regions from our system compared to similar estimates from CT2011_oi and Peylin et al. (2013). The time span of each of these studies is indicated in the table. All units are Pg C yr^{-1}[a].

Region Name	prior flux 2006-2010	This work 2006-2010		This work 2008-2010				CarbonTracker 2006-2010	Peylin et al. (2013) 2006-2010	Niwa et al. (2012) 2006-2008
		Case 1	Case 2	Case 3	Case 4	Case 5	Case 6	CT2011_oi[b]	CTE2013[c]	

1	North American Boreal	-0.01	-0.23	-0.27	-0.25	-0.26	-0.22	-0.19	-0.21	-0.24	-
2	North American Temperate	-0.12	-0.52	-0.60	-0.63	-0.61	-0.56	-0.56	-0.37	-0.42	-
3	South American Tropical	0.02	0.15	0.12	-0.08	0.00	-0.05	0.00	0.18	0.09	-
4	South American Temperate	-0.07	0.11	0.00	-0.01	0.09	0.07	-0.03	0.08	-0.10	-
5	Northern Africa	0.06	0.06	0.05	0.08	-0.06	0.08	0.10	-0.07	0.00	-
6	Southern Africa	-0.05	0.05	0.06	0.10	-0.04	-0.02	0.05	-0.01	-0.01	-
7	Eurasia Boreal	0.03	-1.02	-0.96	-1.11	-1.25	-0.96	-0.92	-1.00	-0.93	-
8	Eurasia Temperate	-0.11	-0.68	-0.33	-0.70	-0.63	-0.44	-0.36	-0.41	-0.33	-
9	Tropical Asia	0.22	0.15	0.19	0.12	0.08	0.17	0.20	0.14	0.22	-
10	Australia	-0.11	-0.03	-0.02	-0.09	-0.12	-0.11	-0.12	-0.01	-0.06	-
11	Europe	-0.09	-0.48	-0.49	-0.50	-0.45	-0.61	-0.67	-0.51	-0.40	-
12	North Pacific Temperate	-0.50	-0.37	-0.38	-0.37	-0.37	-0.39	-0.40	-0.40	-0.41	-
13	West Pacific Tropical	0.00	0.00	0.00	-0.01	0.00	-0.01	-0.01	0.01	0.00	-
14	East Pacific Tropical	0.22	0.31	0.32	0.34	0.34	0.30	0.31	0.33	0.35	-
15	South Pacific Temperate	-0.53	-0.54	-0.62	-0.58	-0.58	-0.58	-0.52	-0.64	-0.60	-
16	Northern Ocean	-0.25	-0.25	-0.27	-0.26	-0.27	-0.25	-0.25	-0.25	-0.30	-
17	North Atlantic Temperate	-0.50	-0.40	-0.40	-0.38	-0.39	-0.46	-0.46	-0.43	-0.47	-

18	Atlantic Tropical	0.14	0.17	0.17	0.17	0.18	0.16	0.16	0.16	0.18	-
19	South Atlantic Temperate	-0.26	-0.17	-0.15	-0.13	-0.11	-0.18	-0.19	-0.18	-0.15	-
20	Southern Ocean	-0.61	-0.31	-0.28	-0.29	-0.28	-0.33	-0.33	-0.37	-0.29	-
21	Indian Tropical	0.13	0.14	0.14	0.14	0.14	0.14	0.14	0.18	0.15	-
22	Indian Temperate	-0.58	-0.66	-0.68	-0.67	-0.70	-0.67	-0.63	-0.70	-0.68	-
23	Non-optimized	0.00	0.00	0.00	0.00	0.00	0.00	0.00	0.00	0.00	-
24	Global Total	-2.99	-4.50	-4.41	-5.12	-5.30	-4.92	-4.68	-4.49	-4.44	-4.46
25	Global Land	-0.25	-2.43	-2.24	-3.07	-3.25	-2.65	-2.50	-2.20	-2.20	-2.67
26	Global Ocean	-2.74	-2.08	-2.16	-2.04	-2.05	-2.27	-2.18	-2.30	-2.24	-1.79
27	Asia (7,8,9)	0.13	-1.56	-1.09	-1.69	-1.80	-1.23	-1.08	-1.27	-1.05	-
28	NH Land (1,2,7,8,11)	-0.32	-2.93	-2.64	-3.20	-3.20	-2.79	-2.70	-2.50	-2.33	-
29	Tropical Land(3,5,9)	0.30	0.36	0.36	0.13	0.02	0.20	0.30	0.26	0.31	-
30	Southern Land (4,6,10)	-0.22	0.13	0.04	0.00	-0.07	-0.06	-0.10	0.05	-0.18	
31	NH Total (1,2,7,8,11,12,16,17)	-1.56	-3.95	-3.69	-4.21	-4.23	-3.89	-3.81	-3.58	-3.52	-
32	Tropical Total(3,5,9,13,14,18,21)	0.79	0.99	0.99	0.77	0.68	0.79	0.90	0.93	0.99	-
33	Southern Total(4,6,10,15,19,20,22)	-2.21	-1.55	-1.70	-1.67	-1.74	-1.82	-1.77	-1.85	-1.91	

[a]All the terrestrial biosphere fluxes are including land uptake and biomass burning emissions, but excluding fossil fuel emissions.

[b]CT2011_oi : this data is derived from http://carbontracker.noaa.gov

[c]CTE2013 is the result of Carbon Tracker Europe (Peters et al., 2010) as presented in Peylin et al., (2013) for the period of 2006-2010

The estimated (a posterior) global CO_2 sinks/sources across 6 sensitivity tests were presented in Table B1, and aggregated to annual mean for TransCom regions. These experiments form a range around the best estimate, given an alternative uncertainty with upper and lower limits of sensitivity tests to the assimilation system. As previously described, the Case 1 was performed the best assimilation on CO_2 source/sink and its results were used to analyze the global carbon flux. Based on the results of annual carbon fluxes in Case 1 (Surface-CONTRAIL), most land regions were estimated to be carbon sinks, characterized by strong sinks in the Eurasia Boreal, Eurasia Temperate, North American Temperate, North American Boreal and Europe; while inverted carbon sources were in Tropical Asia, South America, and Africa (Table B1). The estimated ocean fluxes show the same tendencies as the *a priori* fluxes that East Pacific Tropical, Atlantic Tropical and Indian Tropical Oceans are carbon sources, while the reminders are CO_2 sinks. This distribution of carbon sinks/source is reasonable and quite consistent with other previously published inversion estimates (e.g. Peylin et al. 2013).

Our best global mean CO_2 flux was estimated to be $-4.50^{-4.41}_{-5.30}$ Pg C yr^{-1} (the uncertainty range was derived from Cases 1 to 6) for the period 2006-2010, compared with the global *a priori* flux of -2.99 Pg C yr^{-1}. Note here that the biomass burning emissions (averaged +2.20 Pg C yr^{-1} during the studied period) were included in the inverted flux, but fossil fuel emissions (averaged +8.64 Pg C yr^{-1}) were excluded. For comparison, we included the annual means from CarbonTracker Europe (Peters et al., 2010, quoted as CTE2013) derived from Peylin et al. (2013) and CarbonTracker North America (quoted as CT2011_oi, data downloaded from http://carbontracker.noaa.gov) for the same time period and areas. The CT2011_oi estimates the carbon flux of global terrestrial biosphere and oceans were respectively -2.20 Pg C yr^{-1} and -2.30 Pg C yr^{-1}, while the sink inferred from CTE2013 was estimated to be -2.20 Pg C yr^{-1} on land and -2.24 Pg C yr^{-1} in the ocean. Our inferred global carbon sinks/source ($-4.50^{-4.41}_{-5.30}$ Pg C yr^{-1}) is consistent with that from the CT2011_oi (-4.49 Pg C yr^{-1}) and CTE (-4.44 Pg C yr^{-1}). This consistency can be further represented in the partitioning of the NH land sinks among North America, Asia and Europe. In

North America, our result ($-0.75^{-0.75}_{-0.88}$ Pg C yr^{-1}) generally agrees with CTE2013 (-0.66 Pg C yr^{-1}) and CT2011_oi (-0.58 Pg C yr^{-1}). In Asia, the inverted result is $-1.56^{-1.07}_{-1.80}$ Pg C yr^{-1}, which is within uncertainty and comparable to that of CTE2013 (-1.05 Pg C yr^{-1}) and the CT2011_oi (-1.27 Pg C yr^{-1}). In Europe, our result ($-0.48^{-0.45}_{-0.67}$ Pg C yr^{-1}) is in the range of CT2011_oi (-0.51 Pg C yr^{-1}) and CTE2013 (-0.37 Pg C yr^{-1}).

Also, we found that the addition of CONTRAIL data creates a larger carbon sink in Temperate Asia and the NH land, at the expense of weak ocean uptake. This shifts of the carbon fluxes to a stronger land uptake versus a weaker ocean sink, more in line with the results of Niwa et al. (2013) that there existed a stronger terrestrial uptake (-2.67 Pg C yr^{-1}) and a weaker oceans uptake (-1.79 Pg C yr^{-1}) caused by using CONTRAIL data.

Overall, our global, all-land and all-ocean estimates of the CO_2 flux in this period are reasonable.

Specific comments

P27604, line 17: In realistically, the region number is less than 239. The authors should show actual number to see a number of freedoms. Is it similar to original CTDAS?

Response:

Thank you for this comment that the reviewer is correct. The region number is less than 239 in this study. Similar to the original CTDAS, the actual number assimilated in this system is 156, after excluding 83 scaling factors which associated with a non-existing ecosystems (such as "snowy conifers" in Africa). We corrected this sentence in our revised version (*see page 8 lines 12-14*) as "*The actual region number assimilated in this system is 156, after excluding 83 regions which associated with a non-existing ecosystem (such as "snowy conifers" in Africa).*"

Comment:

P27605, line 24 and Fig. 2a: It is difficult for us to evaluate whether your observation network is suitable or not. The authors should show all

observational sites in Fig. 1.

Response:

We appreciate this comment. Yes, the information about the global surface CO_2 observations is incomplete. Now we completed this content in the revised version and included an additionally table (Table A1) with all global surface sites and their assimilation statistics in SI Appendix A. *See SI Appendix A in pages 51-54.*

SI Appendix A:

Table A1. Summary of the global surface CO_2 observation data assimilated between January 1, 2006 and December 31, 2010. The frequency of continuous data is one data point per day (when available), while discrete surface data point is generally once per week. MDM (model-data-mismatch) is a value assigned to a given site that is meant to quantify our expected ability to simulate observations and used to calculate the innovation X^2 (Inn. X^2) statistic. N denotes that the number is available in the CTDAS. Flagged observations mean the model-minus-observation difference if it exceeds 3 times of the model-data-mismatch and therefore is excluded from assimilation. The bias is the average from posterior residuals (assimilated values – measured values), while the modeled bias is the average from prior residuals (modeled values – measured values). Laboratory abbreviations refer to the description of the GLOBALVIEW product (Masarie and Tans, 1995).

Site	Name	Lat, Lon, Elev.	Lab	N(flagged)	MDM	Inn. X^2	Bias(modeled)
'abp_01d0'	Arembepe, Bahia, Brazil	12.77°S,38.17°W,1m	ESRL	102(0)	3	0.3	-1.18(-1.51)
'abp_26d0'	Arembepe, Bahia, Brazil	12.77°S,38.17°W,1m	IPEN	101(0)	3	0.38	-1.33(-1.67)
'alt_01d0'	Alert, Nunavut, Canada	82.45°N,62.51°W,200m	ESRL	246(0)	1.5	0.43	0.01(0.12)
'alt_06c0'	Alert, Nunavut, Canada	82.45°N,62.51°W,200m	EC	1590(0)	2.5	0.21	0.18(0.27)
'amt_01c3'	Argyle, Maine, United States	45.03°N,68.68°W,50m	ESRL	1571(59)	3	0.98	0.8(0.83)
'amt_01d0'	Argyle, Maine, United States	45.03°N,68.68°W,50m	ESRL	126(0)	1000	0	-0.11(0.14)
'amt_01p0'	Argyle, Maine, United States	45.03°N,68.68°W,50m	ESRL	307(0)	1000	0	0.69(0.52)

asc_01d1'	Ascension Island, United Kingdom	7.92°S,14.42°W,54m	ESRL	413(2)	0.75	0.91	-0.09(-0.14)
'ask_01d0'	Assekrem, Algeria	23.18°N,5.42°E,2728m	ESRL	221(0)	1.5	0.34	-0.11(-0.12)
'azr_01d0'	Terceira Island, Azores, Portugal	38.77°N,27.38°W,40m	ESRL	136(3)	1.5	0.96	0.36(0.39)
'bal_01d0'	Baltic Sea, Poland	55.35°N,17.22°E,3m	ESRL	473(0)	7.5	0.38	0.11(0.23)
'bao_01c3'	Boulder Atmospheric Observatory, Colorado, United States	40.05°N,105.00°W,1584m	ESRL	1482(42)	3	1.02	-0.46(0.11)
'bao_01p0'	Boulder Atmospheric Observatory, Colorado, United States	40.05°N,105.00°W,1584m	ESRL	760(0)	1000	0	-1.78(-1.47)
'bhd_01d0'	Baring Head Station, New Zealand	41.41°S,174.87°E,85m	ESRL	82(0)	1.5	0.3	0.09(0.09)
'bkt_01d0'	Bukit Kototabang, Indonesia	N,100.32°E,864m	ESRL	172(0)	7.5	0.73	5.53(5.51)
'bme_01d0'	St. Davids Head, Bermuda, United Kingdom	32.37°N,64.65°W,30m	ESRL	47(0)	1.5	0.75	0.17(0.21)
'bmw_01d0'	Tudor Hill, Bermuda, United Kingdom	32.27°N,64.88°W,30m	ESRL	143(3)	1.5	0.69	0.19(0.21)
'brw_01c0'	Barrow, Alaska, United States	71.32°N,156.61°W,11m	ESRL	1319(1)	2.5	0.28	0.35(0.55)
'brw_01d0'	Barrow, Alaska, United States	71.32°N,156.61°W,11m	ESRL	227(2)	1.5	0.6	0.12(0.35)
'bsc_01d0'	Black Sea, Constanta, Romania	44.17°N,28.68°E,3m	ESRL	149(7)	7.5	1.33	-4.08(-3.85)
'cba_01d0'	Cold Bay, Alaska, United States	55.21°N,162.72°W,21m	ESRL	290(17)	1.5	1.28	-0.49(-0.42)
cdl_06c30'	Candle Lake, Saskatchewan, Canada	53.99°N,105.12°W,600m	EC	825(9)	3	0.7	0.79(1.5)
cfa_02d0'	Cape Ferguson, Queensland, Australia	19.28°S,147.06°E,2m	CSIRO	96(0)	2.5	0.43	-0.95(-1.19)
'cgo_01d0'	Cape Grim, Tasmania, Australia	40.68°S,144.69°E,94m	ESRL	156(0)	0.75	0.27	-0.06(-0.09)
'cgo_02d0'	Cape Grim, Tasmania, Australia	40.68°S,144.69°E,94m	CSIRO	154(1)	0.75	0.25	-0.12(-0.14)
'chr_01d0'	Christmas Island, Republic of Kiribati	1.70°N,157.17°W,3m	ESRL	192(0)	0.75	1.11	-0.59(-0.65)
'cri_02d0'	Cape Rama,India	15.08°N,73.83°E,60m	CSIRO	33(1)	3	1.4	-1.97(-2.11)
'crz_01d0'	Crozet Island, France	46.45°S,51.85°E,120m	ESRL	217(0)	0.75	0.2	-0.09(-0.14)
'cya_02d0'	Casey, Antarctica, Australia	66.28°S,110.52°E,51m	CSIRO	97(0)	0.75	0.32	-0.28(-0.32)
'egb_06c0'	Egbert, Ontario, Canada	44.23°N,79.78°W,251m	EC	1001(73)	3	1.28	0.88(1.33)
'eic_01d0'	Easter Island, Chile	27.15°S,109.45°W,50m	ESRL	153(0)	7.5	0.02	0.53(0.51)
'esp_06c0'	Estevan Point, British Columbia, Canada	49.38° N ,126.54°W,7m	EC	614(19)	3	0.63	-0.33(-0.25)
'etl_06c0'	East Trout Lake, Saskatchewan, Canada	54.35°N,104.98°W,492m	EC	1063(6)	3	0.51	0.22(0.75)
'fef_03c0'	Fraser, Colorado, United States	39.91°N,105.88°W,2745m	NCAR	2558(158)	3	0.85	-0.43(-0.42)
'gmi_01d0'	Mariana Islands, Guam	13.43°N,144.78°E,3m	ESRL	249(0)	1.5	0.29	-0.09(-0.11)
'gsn_61c0'	Gosan, Republic of Korea	33.15°N,126.12°E,72m	NIER	1274(109)	3	1.99	-1.01(-0.82)

'hba_01d0'	Halley Station, Antarctica, United Kingdom	75.61°S,26.21°W,30m	ESRL	205(0)	0.75	0.22	-0.21(-0.26)
'hdp_03c0'	Hidden Peak (Snowbird), Utah, United States	40.56°N,111.65°W,3351m	NCAR	2285(1)	3	0.27	-0.29(-0.28)
'hpb_01d0'	Hohenpeissenberg, Germany	47.80°N,11.01°E,985m	ESRL	208(0)	7.5	0	2.77(2.86)
'hun_01d0'	Hegyhatsal, Hungary	46.95°N,E,248m	ESRL	232(0)	7.5	0.39	0.35(0.5)
'ice_01d0'	Storhofdi, Vestmannaeyjar, Iceland	63.40°N,20.29°W,118m	ESRL	222(2)	1.5	0.7	-0.39(-0.35)
'izo_01d0'	Izana, Tenerife, Canary Islands, Spain	28.31°N,16.50° W,2372.9m	ESRL	207(0)	1.5	0.72	0.63(0.62)
'key_01d0'	Key Biscayne, Florida, United States	25.67°N,E,3m	ESRL	147(0)	2.5	0.23	-0.04(-0.02)
'kum_01d0'	Cape Kumukahi, Hawaii, United States	19.52°N,154.82°W,3m	ESRL	289(0)	1.5	0.44	-0.21(-0.21)
'kzd_01d0'	Sary Taukum, Kazakhstan	44.06°N,76.82°E,601m	ESRL	167(6)	2.5	1.16	-0.08(0.5)
'kzm_01d0'	Plateau Assy, Kazakhstan	43.25°N,77.88°E,2519m	ESRL	155(2)	2.5	0.96	0.5(0.63)
'lef_01c3'	Park Falls, Wisconsin, United States	45.95°N,90.27°W,472m	ESRL	2267(55)	3	0.87	0.2(0.52)
'lef_01d0'	Park Falls, Wisconsin, United States	45.95°N,90.27°W,472m	ESRL	227(0)	1000	0	0.76(1.09)
'lef_01p0'	Park Falls, Wisconsin, United States	45.95°N,90.27°W,472m	ESRL	1341(0)	1000	0	0.11(0.41)
'llb_06c0'	Lac La Biche, Alberta, Canada	54.95°N,112.45°W,540m	EC	1206(43)	3	1	0.14(0.5)
'lln_01d0'	Lulin,Taiwan	23.47° N,120.87°E,2862m	ESRL	220(20)	7.5	0.99	2.62(2.65)
'lmp_01d0'	Lampedusa, Italy	35.52°N,12.62°E,45m	ESRL	197(0)	1.5	0.91	0.05(0.07)
'maa_02d0'	Mawson Station, Antarctica, Australia	67.62°S,E,32m	CSIRO	87(0)	0.75	0.34	-0.29(-0.32)
'mhd_01d0'	Mace Head, County Galway, Ireland	53.33°N,9.90°W,5m	ESRL	180(0)	2.5	0.18	0(0)
'mid_01d0'	Sand Island, Midway, United States	28.21°N,177.38°W,4m	ESRL	229(0)	1.5	0.74	0.22(0.22)
'mkn_01d0'	Mt. Kenya, Kenya	0.05°S,37.30°E,3897m	ESRL	74(0)	2.5	1.08	1.59(1.56)
'._01c0'	Mauna Loa, Hawaii, United States	19.54°N,155.58°W,3397m	ESRL	1420(4)	0.75	0.55	0.06(0.06)
'mlo_01d0'	Mauna Loa, Hawaii, United States	19.54°N,155.58°W,3397m	ESRL	251(0)	1.5	0.15	0.01(0.02)
'mnm_19c0'	Minamitorishima,Japan	24.29°N,153.98°E,8m	JMA	1624(0)	3	0.76	0.15(0.16)
'mqa_02d0'	Macquarie Island, Australia	54.48°S,158.97°E,12m	CSIRO	114(0)	0.75	0.3	-0.05(-0.07)
'nmb_01d0'	Gobabeb, Namibia	23.58°S,15.03°E,456m	ESRL	142(0)	2.5	0.19	-0.54(-0.58)
'nwr_01d0'	Niwot Ridge, Colorado, United States	40.05°N,105.58°W,3523m	ESRL	226(4)	1.5	0.62	0.21(0.18)
'nwr_01p0'	Niwot Ridge, Colorado, United States	40.05°N,105.58°W,3523m	ESRL	869(31)	1.5	1	0.44(0.43)
'obn_01d0'	Obninsk, Russia	55.11°N,36.60°E,183m	ESRL	68(5)	7.5	0.64	-1.51(-1.29)
'oxk_01d0'	Ochsenkopf, Germany	50.03°N,11.80°E,1022m	ESRL	139(10)	2.5	1.32	-0.18(-0.11)
'pal_01d0'	Pallas-Sammaltunturi, GAW Station, Finland	67.97°N,24.12°E,560m	ESRL	225(3)	2.5	0.74	0.06(0.32)

'poc_01d1'	Pacific Ocean, N/A	0.39°S,132.32°W,10m	ESRL	853(10)	0.75	0.79	-0.07(-0.1)
'psa_01d0'	Palmer Station, Antarctica, United States	64.92°S,64.00°W,10m	ESRL	247(0)	0.75	0.43	-0.27(-0.35)
'pta_01d0'	Point Arena, California, United States	38.95°N,123.74°W,17m	ESRL	200(0)	7.5	0.34	-2.19(-2.08)
'rpb_01d0'	Ragged Point, Barbados	13.17°N,59.43°W,45m	ESRL	227(0)	1.5	0.57	-0.15(-0.17)
'ryo_19c0'	Ryori,Japan	39.03°N,141.82°E,260m	JMA	1663(48)	3	0.9	0.46(0.69)
'sdz_01d0'	Shangdianzi, China	40.39°N,117.07°E,287m	CMA/ESRL	60(15)	3	1.18	0.15(0.18)
'sey_01d0'	Mahe Island, Seychelles	4.67°S,55.17°E,3m	ESRL	221(5)	0.75	0.77	-0.07(-0.08)
'sgp_01d0'	Southern Great Plains, Oklahoma, United States	36.80°N,97.50°W,314m	ESRL	225(13)	2.5	1.28	-0.51(-0.14)
'shm_01d0'	Shemya Island, Alaska, United States	52.72°N,174.10°E,40m	ESRL	149(0)	2.5	1.02	-0.11(-0.05)
'smo_01c0'	Tutuila, American Samoa	14.25°S,170.56°W,42m	ESRL	1598(0)	0.75	0.49	0.1(0.09)
'smo_01d0'	Tutuila, American Samoa	14.25°S,170.56°W,42m	ESRL	239(0)	1.5	0.16	-0.06(-0.09)
'snp_01c3'	Shenandoah National Park, United States	38.62°N,78.35°W,1008m	ESRL	1237(98)	3	1.5	-0.14(0.04)
'spl_03c0'	Storm Peak Laboratory (Desert Research Institute), United States	40.45°N,106.73°W,3210m	NCAR	1874(14)	3	0.62	-0.68(-0.69)
'spo_01d0'	South Pole, Antarctica, United States	89.98°S,24.80°W,2810m	ESRL	238(0)	1.5	0.04	-0.16(-0.2)
'stm_01d0'	Ocean Station M, Norway	66.00°N,2.00°E,0m	ESRL	343(3)	1.5	0.68	0.16(0.28)
'str_01p0'	Sutro Tower, San Francisco, California, United States	37.76°N,122.45°W,254m	ESRL	698(0)	1000	0	-0.27(-0.14)
'sum_01d0'	Summit, Greenland	72.58°N,38.48°W,3238m	ESRL	248(0)	1.5	0.47	0.16(0.21)
'syo_01d0'	Syowa Station, Antarctica, Japan	69.00°S,39.58°E,11m	ESRL	114(0)	0.75	0.22	-0.24(-0.28)
'tap_01d0'	Tae-ahn Peninsula, Republic of Korea	36.73°N,126.13°E,20m	ESRL	181(3)	7.5	0.6	1.82(2.13)
'tdf_01d0'	Tierra Del Fuego, Ushuaia, Argentina	54.87°S,68.48°W,20m	ESRL	117(0)	0.75	0.74	-0.36(-0.42)
'thd_01d0'	Trinidad Head, California, United States	41.05°N,124.15°W,107m	ESRL	232(21)	2.5	1.33	-1.49(-1.56)
'uta_01d0'	Wendover, Utah, United States	39.90°N,113.72°W,1320m	ESRL	220(11)	2.5	0.76	0.65(0.98)
'uum_01d0'	Ulaan Uul, Mongolia	44.45°N,111.10°E,914m	ESRL	231(5)	2.5	1.17	0.1(0.28)
'wbi_01c3'	West Branch, Iowa, United States	41.72°N,91.35°W,242m	ESRL	1801(141)	3	1.21	0.22(0.64)
'wbi_01p0'	West Branch, Iowa, United States	41.72°N,91.35°W,242m	ESRL	845(0)	1000	0	0.36(0.81)
'wgc_01c3'	Walnut Grove, California, United States	38.27°N,121.49°W,0m	ESRL	1736(132)	3	1.22	-0.59(-0.46)
'wgc_01p0'	Walnut Grove, California, United States	38.27°N,121.49°W,0m	ESRL	878(0)	1000	0	-4.55(-4.41)
'wis_01d0'	WIS Station, Negev Desert, Israel	31.13°N,34.88°E,400m	ESRL	239(1)	2.5	0.62	-0.1(-0.15)

'wkt_01c3'	Moody, Texas, United States	31.31°N,97.33°W,251m	ESRL	2124(24)	3	0.74	0.11(0.11)
'wkt_01d0'	Moody, Texas, United States	31.31°N,97.33°W,251m	ESRL	168(0)	1000	0	0.15(0.2)
'wkt_01p0'	Moody, Texas, United States	31.31°N,97.33°W,251m	ESRL	979(0)	1000	0	-0.42(-0.45)
'wlg_01d0'	Mt. Waliguan, Peoples Republic of China	36.29°N,100.90°E,3810m	CMA/ESRL	254(19)	1.5	0.83	-0.1(-0.14)
'yon_19c0'	Yonagunijima, Japan	24.47°N,123.02°E,30m	JMA	1684(3)	3	0.78	1.53(1.67)
'zep_01d0'	Ny-Alesund, Svalbard, Norway and Sweden	78.90°N,11.88°E,475m	ESRL	217(2)	1.5	0.75	0.61(0.8)

Comment:

P27608, line 7: The authors should show land use maps (MODIS) in Case 6.

Response:

Thank you for this comment. The land use maps (MODIS) & associated text was added in the Supporting Information Appendix C (*see pages 58-59*).

"Supporting Information Appendix C:

Table C1. The MODIS land use categories converted to the corresponded Olson, et al. (1985) land types table

	IGBP	Olson, et al. (1985)
0	Water Bodies	18 Non-optimized areas (ice, polar desert,inland seas)
1	Evergreen Needleleaf Forest	1 Conifer Forest
2	Evergreen Broadleaf Forest	5 Tropical Forest
3	Deciduous Needleleaf Forest	1 Conifer Forest
4	Deciduous Broadleaf Forest	2 Broadleaf Forest

5	Mixed Forest	3 Mixed Forest
6	Closed Shrublands	13 Shrub/Tree/Suc
7	Open Shrubland	4 Grass/Shrub
8	Woody Savannas	8 Fields/Woods/Savanna
9	Savannas	13 Shrub/Tree/Suc
10	Grasslands	4 Grass/Shrub
11	Permanent Wetlands	11 Wetland
12	Croplands	14 Crops
13	Urban and Built-up	18 Non-optimized areas (ice, polar desert,inland seas)
14	Cropland/Natural Vegetation Mosaic	14 Crops
15	Snow and Ice	18 Non-optimized areas (ice, polar desert,inland seas)
16	Barren or Sparsely Vegetated	12 Deserts

To assess the impact of land cover map on carbon flux, we used MODIS land cover data (MCD12Q1 version 051 of year 2005) in place of map of Olson et al. (1985). The MODIS land cover map was re-sampled into a 1×1 degree spatial resolution by selecting the pixels with maximum area, and then was converted into Olson et al. (1985) land types. The conversion strategy from MODIS IGBP categories into Olson et al. (1985) land classification are summarized in Table C1. The processed MODIS data are showed in Figure C1. We found that this land cover data are very different from that of Olson et al. (1985), which could produce large changes in inverted carbon flux.

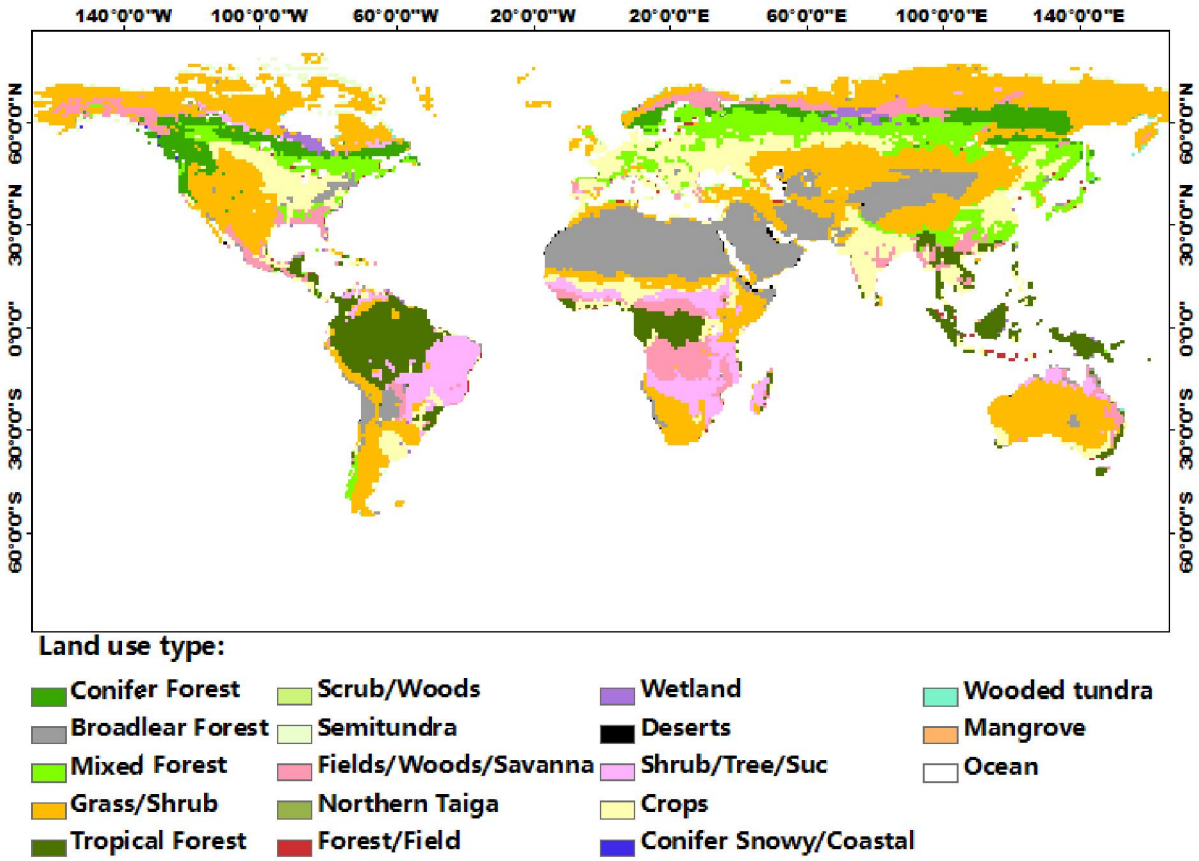

Figure C1.The land use maps (MODIS) used in Case 6"

Comment:

P27608, line 20 and table 1: To evaluate the authors' transport model performance including prior CO2 flux, it is better to compare not only

assimilated CO2 but also simulated CO2. The results could indicate some information about prior flux. Also non-Asian observational data (not all but representative sites) are available for such purpose.

Response:

Thank you for this comment. We agree that the information about the modeled CO_2 concentrations ie very important to evaluate the transport model performance. We updated Table 1 with non-assimilated CO_2 in the revised version (*See revised Table 1 in Pages 32-33). And also, a* additionally table (Table A1) with all global surface sites and their assimilation statistics in SI Appendix A (*See SI Appendix A in pages 51-54).*

Table 1 Summary of the 14 Asian surface CO_2 observation data assimilated between January 1, 2006 and December 31, 2010. The frequency of continuous data is one per day (when available), while discrete surface data point is generally once per week. MDM (model-data-mismatch) is a value assigned to a given site that is meant to quantify our expected ability to simulate observations and used to calculate the innovation X^2 (Inn. X^2) statistic. N denotes that the number is available in the CTDAS. Flagged observations mean a model-minus-observation difference that exceeds 3 times of the model-data-mismatch and were therefore excluded from assimilation. The bias is the average from posterior residuals (assimilated values – measured values), while the modeled bias is the average from prior residuals (modeled values – measured values)

Site	Name	Lat, Lon, Elev.	Lab	N(flagged)	MDM	Inn. X^2	Bias(modeled)
Discrete samples in Asia:							
1 WLG	Waliguan,China	36.29°N,100.90°E,3810m	CMA/ESRL	254(19)	1.5	0.83	-0.10(-0.14)

2 BKT	Bukit Kototabang,Indonesia	0.20°S,100.312°E,864m	ESRL	172(0)	7.5	0.73	5.53(5.51)
3 WIS	Sede Boker,Israel	31.13°N,34.88°E,400m	ESRL	239(1)	2.5	0.62	-0.10(-0.15)
4 KZD	Sary Taukum,Kazakhstan	44.45°N,77.57°E,412m	ESRL	167(6)	2.5	1.16	-0.08(0.50)
5 KZM	Plateau Assy,Kazakhstan	43.25°N ,77.88°E,2519m	ESRL	155(2)	2.5	0.96	0.50(0.63)
6 TAP	Tae-ahn Peninsula,Korea	36.73°N,126.13°E,20m	ESRL	181(3)	7.5	0.60	1.82(2.13)
7 UUM	Ulaan Uul,Mongolia	44.45°N,111.10°E,914m	ESRL	231(5)	2.5	1.17	0.10(0.28)
8 CRI	Cape Rama,India	15.08°N,73.83°E,60m	CSIRO	33(1)	3	1.40	-1.97(-2.11)
9 LLN	Lulin,China	23.47°N,120.87°E,2867m	ESRL	220(20)	7.5	0.99	2.62(2.65)
10 SDZ	Shangdianzi, China	40.39°N,117.07°E,287m	CMA/ESRL	60(15)	3	1.18	0.15(0.18)
Continuous samples in Asia:							
11 MNM	Minamitorishima,Japan	24.29°N,153.98°E,8m	JMA	1624(0)	3	0.76	0.15(0.16)

12 RYO	Ryori,Japan	39.03°N,141.82°E,260m	JMA	1663(48)	3	0.90	0.46(0.69)
13 YON	Yonagunijima, Japan	24.47°N,123.02°E,30m	JMA	1684(3)	3	0.78	1.53(1.67)
14 GSN	Gosan, Republic of Korea	33.15°N,126.12°E,72m	NIER	1274(109)	3	1.99	-1.01(-0.82)

Comment:

P27613, line 1 and table 3: In this table, the authors should add results of the same period (2008 – 2010) in Case 1 and 2 to compare similar condition and rewrite this section (3.2.3).

Response:

Thank you for this comment. In fact, the comparison of the results from Cases 1 and 2 with other 4 inversion experiments is not our purpose of this study as we aimed at providing alternative range to the inverted Asia carbon flux. However, we agree with that it is very important to compare the results for the same period (2008 – 2010) from Cases 1 and 2. We updated this section in our revised version accordingly. *See page 18 lines 5-10*: "*The time spans are different among these 6 tests: Case 1 (surface-CONTRAIL) and Case 2 (surface-Only) run for the period 2006-2010 (2000-2005 servers as a spin-up period), while Cases 3 to 6 run for the period 2008-2010. To compare other alternative sensitivity estimates for the same period from 2008 to 2010, we calculated this three-year average of annual Asia CO_2 fluxes (2008-2010) from all the 6 tests to be −1.61, −1.15, −1.69, −1.80, −1.23 and −1.07 PgC yr^{-1}, respectively*."

Comment:

P27614, line 24-: I consider the difference is affected by strength of vertical mixing (maybe cumulus convection in tropical region) in transport model. The authors should comment it.

Response:

We agree to this point that the vertical mixing in transport model could be an important contributor to the error reduction, with and without the CONTRAIL data. We added these difference analyses in the revised version (*see page 20 lines 6-11*): "*This difference in uncertainty reduction likely results from the differences in revision system design between these two studies, of which vertical mixing represented in transport model, the CO_2 network used in system and covariance assigned to prior fluxes are typically most important"*. And also, we discussed the strength of vertical mixing in section 3.1 (*see page 13 line 18 to page 14 line 13*).

"3.1 CO_2 concentration simulations

First we checked the accuracy of the model simulation using the surface CO_2 concentration observations and CONTRAIL aircraft CO_2 measurements. Figure 3a shows the comparison of modeled (both prior and posterior) CO_2 concentration with measurements at the discrete surface site of Mt. Waliguan (WLG, located at 36.29° N, 100.90° E). Note that the prior CO_2 concentrations here are not really based on a-priori fluxes only, as they are a forecast started from the CO_2 mixing ratio field that contains all the already optimized fluxes (1,…, n-1) that occurred before the current cycle of the data assimilation system (n). So these prior mole fractions only contain five weeks of recent un-optimized fluxes and constitute our 'first-guess' of atmospheric CO_2 for each site. For the WLG site, the comparison of the surface CO_2 time series shows that the modeled (both prior and posterior) CO_2 concentration is in general agreement with observed data during the period 2006-2010 (correlation coefficient R=0.87), although the modeled result still could not adequately reproduce all the observed CO_2 seasonal variations. The posterior annual model-observation mismatch of this distribution is −0.10±1.25, with 0.07±1.50 ppm bias for the summer period (June-July-August) and 0.02±0.80 ppm bias for the winter period (December-January-February). Over the full study period, the WLG modeled mole fractions exhibit good agreement with the observed CO_2 time series and the changes in inferred mixing ratios/flux are within the specified uncertainties in our inversion system, an important prerequisite for a good flux estimate.

We also checked the inversion performance in the free troposphere in addition to the surface CO_2. Figures 3b, 3c and 3d show the comparison between measured and modeled (both prior and posterior) mixing ratios in the free troposphere during the period 2006-2010 in the region covering 136-144°N, 32-40°E for 3 vertical bins (475–525, 375–425, 225–275 hPa). The observed vertical CO_2 patterns were reasonably reproduced by our model, with high correlation coefficient (R = 0.95, 0.94 and 0.93 for 475–525, 375–425, 225–275 hPa, respectively) between CONTRAIL and modeled CO_2. The observed low vertical gradients for flight sections in 3 vertical bins (475–525, 375–425, 225–275 hPa) at northern mid-latitudes (32-40°E) were well captured by the model (both prior and posterior), indicating the transport model can reasonably produce the vertical structure of observations. We also found that the observed CO_2 concentration

profiles were modeled better after assimilation than before (modelled –observed = −0.01±1.18 ppm for a-priori and 0.05±1.25 ppm for posterior), although our inverted (posterior) mole fractions still could not adequately reproduce the high values in winter (December-January-February) and the low values in summer (June-July-August). This mismatch of CO_2 seasonal amplitude suggests that our inverted (posterior) CO_2 surface fluxes do not catch the peak of terrestrial carbon exchange well. Previous studies have also found this seasonal mismatch, which may correlate with atmospheric transport, and has already been identified as a shortcoming in most inversions (Peylin et al., 2013; Saeki et al., 2013; Stephens et al., 2007; Yang et al., 2007). Overall, the agreement between the modeled and measurements is fairly good and consistent with previously known behavior in the CarbonTracker systems, derived mostly from North American and European continuous sites."

Comment:

P27615, line 1-: The fact that authors used BKT site in their analysis is consistent to the low error reduction rate in Tropical Asia region. I consider observation network is also important factor to evaluate error reduction.

Response:

Indeed, many factors could affect the error reduction rate in the Tropical Asia region, such as the different observations used in the inversion. We have modified our draft accordingly and the impact of observation network on error reduction was discussed in the revised version (*see page 20 lines 6-10*). "*This* difference in uncertainty reduction likely results from the differences in revision system design between these two studies, of which vertical mixing represented in transport model, the CO_2 network used in system and covariance assigned to prior fluxes are typically most important."

Comment:

P27616, line 6- and table 6: The authors should compare not only averaged Asian CO_2 fluxes but also time series of them. As there may be large inter-annual variation in Asian CO_2 fluxes and it is hard to obtain meaningful results by comparing only averaged fluxes.

Response:

Thank you for this comment. In fact, most results shown in **Table 6** coverage different time periods, which make it hard to compare inter-annual variation in Asian CO_2 flux directly. Now we updated this Table with the same time period for the IAVs' comparison of CO_2 fluxes. *See Tables 6 & 7 in pages 39 - 40 and associated text in page 21 line 14 to page 22 line 13*.

Table 6 Comparison of the inverted Asia carbon sinks from this study with previous studies (in Pg C yr^{-1})

Reference	Period	Boreal Eurasia	Temperate Eurasia	Tropical Asia	Asia	Remarks
This study	2006-2010	-1.02±0.91	-0.68±0.70	+0.15±0.28	-1.56±1.18	Surface-CONTRAIL
[Gurney *et al.*,2003]	1992-1996	-0.59±0.52	-0.60±0.67	+0.67±0.70	-0.52±0.65	–
[Maki *et al.*,2010]	2001-2007	-1.46±0.41	0.96±0.59	-0.15±0.44	-0.65±0.49	CNTL experiments
CTE2013[a]	2006-2010	-0.93±1.15	−0.33±0.56	+0.22±0.20	-1.05±1.29	Focused on North America and Europe
CT2011_oi[b]	2006-2010	-1.00	–0.41	+0.14	–1.27	Focused on North America
[Niwa *et al.*,2012][c]	2006-2008	-	-	+0.45±0.19	-	GVCT

[a]CTE2013 is the result of Carbon Tracker Europe in the pylin et al., (2013) for the period of 2006-2010

[b]CT2011_oi : this data is derived from http://carbontracker.noaa.gov; data did not provide the uncertainties

[c] GVCT : together use GLOBALVIEW and CONTRAIL CO_2 observation data to perform inversion

Table 7 Comparison of IAVs of the terrestrial ecosystem carbon fluxes in Asia during 2006-2010 from this study with previous studies. These fluxes in Pg C yr^{-1} include biomass burning emissions but exclude fossil fuel emissions

Reference	year	Asia	Boreal Eurasia	Eurasia temperate	tropical Asia
This study	2006	-1.16	-0.93	-0.60	0.37
	2007	-1.83	-1.17	-0.80	0.14
	2008	-1.71	-0.96	-0.66	-0.09
	2009	-1.80	-1.04	-0.88	0.12
	2010	-1.31	-1.01	-0.49	0.19
CTE2013	2006	-0.92	-0.93	-0.40	0.41
	2007	-1.14	-0.88	-0.44	0.18
	2008	-1.39	-1.07	-0.33	0.00
	2009	-0.87	-0.78	-0.34	0.25
	2010	-0.86	-1.02	-0.12	0.27
CT2011_oi	2006	-0.99	-0.78	-0.46	0.25
	2007	-1.25	-0.92	-0.46	0.13
	2008	-1.51	-1.13	-0.38	0.00
	2009	-1.40	-0.99	-0.51	0.10
	2010	-1.15	-1.16	-0.22	0.23

"Comparisons of our inverted CO_2 flux with previous studies are summarized in Table 6. In Boreal Eurasia, our inferred land flux (−1.02 Pg C yr^{-1}) is higher than Gurney et al. (2003) (−0.59 Pg C yr^{-1} during 1992-1996), but close to Maki et al. (2010) (−1.46 Pg C yr^{-1} during 2001-2007), CTE2013 (−0.93 Pg C yr^{-1}) and CT2011_oi (−1.00 Pg C yr^{-1}, downloaded from http://carbontracker.noaa.gov). In Temperate Eurasia, our inverted flux is −0.68 Pg C yr^{-1}, which is well consistent with Gurney et al. (2003) (−0.60 Pg C yr^{-1}), but higher than CTE2013 (−0.33 Pg C yr^{-1}) and CT2011_oi (−0.41 Pg C yr^{-1}) even though we used a similar inversion framework. One reason of this discrepancy is likely that different zoomed regions were configured in the inversion system. Another main factor is likely the inclusion

of CONTRAIL largely impacts on our Temperate Eurasia's carbon estimates. In Tropical Asia, our estimate is +0.15 Pg C yr^{-1}, which is in the range of Niwa et al.(2012) (+0.45 Pg C yr^{-1}) and Patra et al.(2013) (−0.104 Pg C yr^{-1}), both including aircraft CO_2 measurements in their inversion modeling, and very close to the CTE2013 (+0.22 Pg C yr^{-1}) and CT2011_oi (+0.14 Pg C yr^{-1}). The estimated total Asian terrestrial carbon sink is −1.56 Pg C yr^{-1}, which is close to the CTE2013 (−1.05 Pg C yr^{-1}) and CT2011_oi (−1.27 Pg C yr^{-1}). The IAVs comparison between the results from this study and from CTE2013/CT2011_oi is also presented in Table 7 (different from IAV in Section 3.2.2, these results include biomass burning emissions). The IAVs are different between approaches. In 2007, there was a moderate Asian CO_2 sink in CTE2013 and CT2011_oi, while the results from this study show Asian was the highest carbon uptake during this study period, corresponding to strong CO_2 sinks in Eurasia Temperate and Eurasia Boreal areas. In 2008, Asian was the strongest terrestrial CO_2 sink from CTE2013 and CT2011_oi, while from our estimates that the sink in 2008 in Asian was weaker than that in 2007. In Asian, 2009 was a lower-than-average land sink in CTE2013 and a normal carbon sink in CT2011_oi, while from our results 2009 was the second strongest carbon uptake year. This discrepancy likely stems from the additions of Asia sites and CONTRAIL data in this study. Compared to previous findings, our updated estimation with these additional data seems to support a larger Asian carbon sink over the past decade."

References added

Gurney, K. R., D. Baker, P. Rayner, and S. Denning (2008), Interannual variations in continental-scale net carbon exchange and sensitivity to observing networks estimated from atmospheric CO2 inversions for the period 1980 to 2005, *Global Biogeochem. Cycles*, *22*, 3025.

Gurney, K. R., R. M. Law, A. S. Denning, P. J. Rayner, D. Baker, P. Bousquet, L. Bruhwiler, Y. H. CHEN, P. Ciais, and S. Fan (2003), TransCom 3 CO2 inversion intercomparison: 1. Annual mean control results and sensitivity to transport and prior flux information, *Tellus B*, *55*(2), 555-579.

Gurney, K. R., R. M. Law, A. S. Denning, P. J. Rayner, B. C. Pak, D. Baker, P. Bousquet, L. Bruhwiler, Y. H. Chen, and P. Ciais (2004), Transcom 3 inversion intercomparison: Model mean results for the estimation of seasonal carbon sources and sinks, *Global Biogeochem. Cycles*, *18*(1).

Maki, T., M. Ikegami, T. Fujita, T. Hirahara, K. Yamada, K. Mori, A. Takeuchi, Y. Tsutsumi, K. Suda, and T. Conway (2010), New

technique to analyse global distributions of CO2 concentrations and fluxes from non‐processed observational data, *Tellus B*, *62*(5), 797-809.
Mohammat, A., X. Wang, X. Xu, L. Peng, Y. Yang, X. Zhang, R. B. Myneni, and S. Piao (2012), Drought and spring cooling induced recent decrease in vegetation growth in Inner Asia, *Agr Forest Meteorol*.
Niwa, Y., T. Machida, Y. Sawa, H. Matsueda, T. J. Schuck, C. A. M. Brenninkmeijer, R. Imasu, and M. Satoh (2012), Imposing strong constraints on tropical terrestrial CO2 fluxes using passenger aircraft based measurements, *Journal of Geophysical Research: Atmospheres*, *117*(D11), D11303, doi:10.1029/2012jd017474.
Patra, P., J. Canadell, R. Houghton, S. Piao, N.-H. Oh, P. Ciais, K. Manjunath, A. Chhabra, T. Wang, and T. Bhattacharya (2013), The carbon budget of South Asia, *Biogeosciences*, *10*, 513-527.
Patra, P., Y. Niwa, T. Schuck, C. Brenninkmeijer, T. Machida, H. Matsueda, and Y. Sawa (2011), Carbon balance of South Asia constrained by passenger aircraft CO2 measurements, *Atmos. Chem. Phys*, *11*(9), 4163-4175.
Peters, W., A. R. Jacobson, C. Sweeney, A. E. Andrews, T. J. Conway, K. Masarie, J. B. Miller, L. M. P. Bruhwiler, G. Petron, and A. I. Hirsch (2007), An atmospheric perspective on North American carbon dioxide exchange: CarbonTracker, *Proceedings of the National Academy of Sciences*, *104*(48), 18925.
Peters, W., M. Krol, G. Van der Werf, S. Houweling, C. Jones, J. Hughes, K. Schaefer, K. Masarie, A. Jacobson, and J. Miller (2010), Seven years of recent European net terrestrial carbon dioxide exchange constrained by atmospheric observations, *Global Change Biol*, *16*(4), 1317-1337.
Peylin, P., R. Law, K. Gurney, F. Chevallier, A. Jacobson, T. Maki, Y. Niwa, P. Patra, W. Peters, and P. Rayner (2013), Global atmospheric carbon budget: results from an ensemble of atmospheric CO 2 inversions, *Biogeosciences Discussions*, *10*(3), 5301-5360.
Stephens, B. B., K. R. Gurney, P. P. Tans, C. Sweeney, W. Peters, L. Bruhwiler, P. Ciais, M. Ramonet, P. Bousquet, and T. Nakazawa (2007), Weak northern and strong tropical land carbon uptake from vertical profiles of atmospheric CO2, *Science*, *316*(5832), 1732-1735.
Valsala, V., Y. K. Tiwari, P. Pillai, M. Roxy, S. Maksyutov, and R. Murtugudde (2013), Intraseasonal variability of terrestrial biospheric CO2 fluxes over India during summer monsoons, *Journal of Geophysical Research: Biogeosciences*.
Yang, Z., R. Washenfelder, G. Keppel-Aleks, N. Krakauer, J. Randerson, P. Tans, C. Sweeney, and P. Wennberg (2007), New constraints on Northern Hemisphere growing season net flux, *Geophys Res Lett*, *34*(12), L12807.
Yu, G. R., X. J. Zhu, Y. L. Fu, H. L. He, Q. F. Wang, X. F. Wen, X. R. Li, L. M. Zhang, L. Zhang, and W. Su (2013), Spatial patterns and climate drivers of carbon fluxes in terrestrial ecosystems of China, *Global Change Biol*, *19*(3), 798-810.